AGU PUBLICATIONS

Geophysical Research Letters

RESEARCH LETTER
10.1002/2015GL063259

Key Points:
- Crustal and upper mantle structures are characterized in Red Sea and Afar
- Magmatic processes are currently modifying the crust of the Red Sea flanks
- Rift-flank magmatism can persist after breakup

Supporting Information:
- Text S1
- Figure S1
- Figure S2

Correspondence to:
F. Korostelev,
felicie.korostelev@gmail.com

Citation:
Korostelev, F., et al. (2015), Magmatism on rift flanks: Insights from ambient noise phase velocity in Afar region, *Geophys. Res. Lett.*, *42*, doi:10.1002/2015GL063259.

Received 26 JAN 2015
Accepted 2 MAR 2015
Accepted article online 7 MAR 2015

Magmatism on rift flanks: Insights from ambient noise phase velocity in Afar region

Félicie Korostelev[1,2], Cornelis Weemstra[3], Sylvie Leroy[1,2], Lapo Boschi[1,2], Derek Keir[4], Yong Ren[5], Irene Molinari[6], Abdulhakim Ahmed[1,2,7], Graham W. Stuart[5], Frédérique Rolandone[1,2], Khaled Khanbari[8], James O. S. Hammond[9], J. M. Kendall[10], Cécile Doubre[11], Ismail Al Ganad[12], Berhe Goitom[13], and Atalay Ayele[14]

[1]Sorbonne Universités, UPMC Université Paris 06, UMR 7193, Institut des Sciences de la Terre Paris, Paris, France, [2]CNRS, UMR 7193, Institut des Sciences de la Terre Paris, Paris, France, [3]Department of Geoscience and Engineering, Delft University of Technology, Delft, Netherlands, [4]National Oceanography Centre Southampton, University of Southampton, Southampton, UK, [5]School of Earth and Environment, University of Leeds, Leeds, UK, [6]Istituto Nazionale di Geofisica e Vulcanologia, Rome, Italy, [7]Seismological and Volcanological Observatory Center, Dhamar, Yemen, [8]Sana'a University, Remote Sensing and GIS Center, Sana'a, Yemen, [9]Imperial College London, London, UK, [10]University of Bristol, Bristol, UK, [11]Institut de Physique du Globe de Strasbourg; UMR 7516, Université de Strasbourg/EOST, CNRS, Strasbourg, France, [12]Yemen Geological Survey and Mineral Resources Board, Sana'a, Yemen, [13]School of Earth Sciences, University of Bristol, Bristol, UK, [14]Institute of Geophysics, Space Science and Astronomy, Addis Ababa University, Addis Ababa, Ethiopia

Abstract During the breakup of continents in magmatic settings, the extension of the rift valley is commonly assumed to initially occur by border faulting and progressively migrate in space and time toward the spreading axis. Magmatic processes near the rift flanks are commonly ignored. We present phase velocity maps of the crust and uppermost mantle of the conjugate margins of the southern Red Sea (Afar and Yemen) using ambient noise tomography to constrain crustal modification during breakup. Our images show that the low seismic velocities characterize not only the upper crust beneath the axial volcanic systems but also both upper and lower crust beneath the rift flanks where ongoing volcanism and hydrothermal activity occur at the surface. Magmatic modification of the crust beneath rift flanks likely occurs for a protracted period of time during the breakup process and may persist through to early seafloor spreading.

1. Introduction

During the breakup of continents, stretching and thinning of the plate commonly causes decompression melting and volcanism. In the resultant magmatically active rift valleys it is widely thought that extension is initially accommodated mainly by border faulting and progressively localizes to relatively narrow axial volcanic segments as the rift valley widens [e.g., *Ebinger and Casey*, 2001]. However, it is becoming increasingly more recognized that magma intrusion and volcanism can occur on the rift flanks at an early stage of rifting [e.g., *Maccaferri et al.*, 2014]. These rift flank magmatic systems accommodate extension through diking [*Rooney et al.*, 2014], and thermally and compositionally modify the lithosphere [*Daniels et al.*, 2014]. Despite the importance of magmatic processes during continental extension, we have few constraints on their spatial and temporal variability. In order to address this issue, we use ambient seismic noise tomography to image the Rayleigh wave phase velocity structure of the crust in a region of late-stage breakup at the conjugate margins of the southern Red Sea in Afar and Yemen.

Geochronological constraints in Ethiopia suggest rifting began 29–31 Ma on the western Afar margin [e.g., *Ayalew et al.*, 2006; *Wolfenden et al.*, 2005] (Figure 1), approximately coeval with ~35 Ma faulting along large portions of the Gulf of Aden to the east [*Leroy et al.*, 2010]. Rifting was associated with the development of large offset border faults that currently define ~2000–3000 m of relief between the submarine Red Sea and subaerial Afar depression with the uplifted Ethiopian and Yemeni plateaus [*Wolfenden et al.*, 2004]. Extension is thought to have occurred above warm mantle with a potential temperature of ~1450° [*Rooney et al.*, 2012], associated with voluminous flood basalts on the Ethiopian and Yemeni plateaus synchronous with the onset of extension [*Wolfenden et al.*, 2004], and associated with ongoing magmatism [*Ferguson et al.*, 2013]. At ~21–23 Ma, magmatism occurred through dike intrusions along most of the eastern margin of the Red Sea [*Bosworth et al.*, 2005]. Magmatism on the rift flanks is ongoing, with the Quaternary

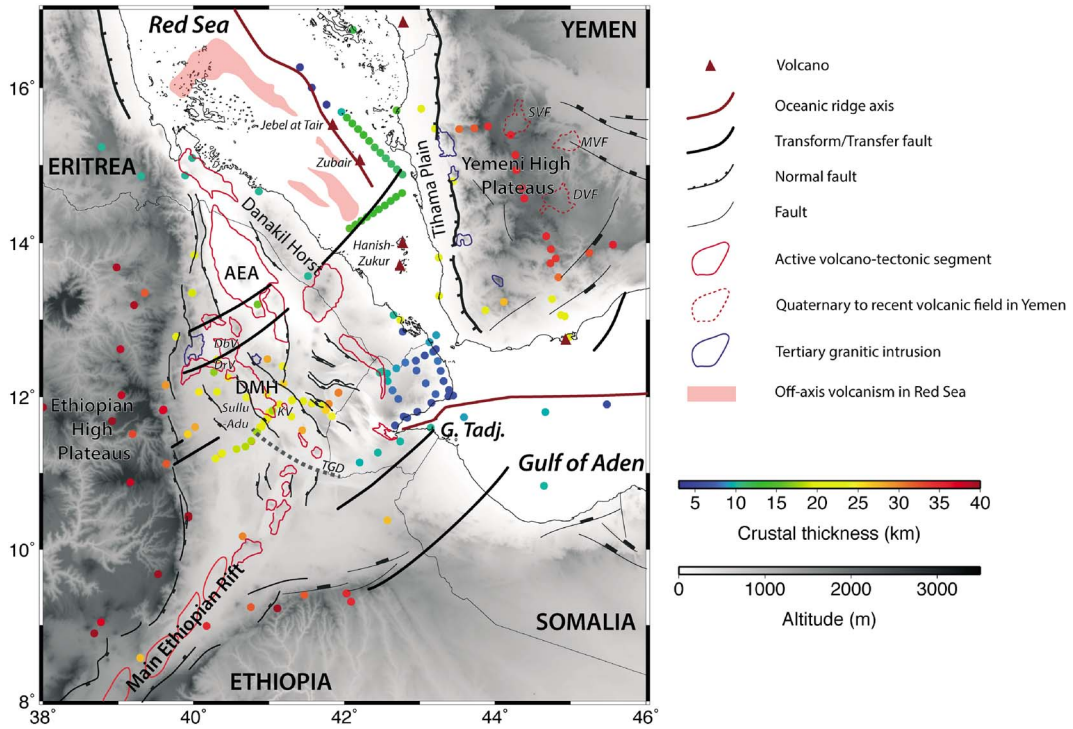

Figure 1. Structure of the Afar and southern Red Sea region. The crustal thicknesses are displayed by colored dots and based on the Moho depths, which are obtained from *Egloff et al.* [1991], *Tramontini and Davies* [1969], *Drake and Girdler* [1964], *Prodehl and Mechie* [1991], *Laughton and Tramontini* [1969], *Ruegg* [1975], *Hammond et al.* [2011], *Ahmed et al.* [2013], and *Reed et al.* [2014]. Structures are modified from *Ebinger et al.* [2008] and *Stab et al.* [2014]. Bathymetry is not represented. DMH: Dabbahu-Manda-Hararo volcano-tectonic segment; AEA: Afdera-Erta'Ale volcano-tectonic segment; G. Tadj.: Gulf of Tadjura; DbV: Dabbahu Volcano; DrV: Durrie Volcano; KV: Kurub Volcano; TGD: Tendaho-Goba'ad Discontinuity; SVF: Sana'a volcanic field; MVF: Marib volcanic field; and DVF: Dhamar volcanic field.

to Recent volcanic centers of Sana'a, Dhamar, and Marib located in Yemen [*Manetti et al.*, 1991; *Korostelev et al.*, 2014]. In addition, thermal hot springs are present along the conjugate southern Afar margin [*Keir et al.*, 2009]. Magma intrusion and volcanism is also common within the rift valley. Since ~10 Ma in Afar, extension via diking progressively localized to the rift axis [e.g., *Wolfenden et al.*, 2005; *Rooney et al.*, 2011], with the current locus of strain being ~70 km long, ~20 km wide axial volcanic segments such as the Dabbahu-Manda-Hararo segment in central west Afar [e.g., *Hayward and Ebinger*, 1996]. Here episodic intrusion of dikes fed from crustal magma chambers at both the segments centers and tips accommodates the majority of extension [e.g., *Keir et al.*, 2009; *Grandin et al.*, 2010, 2011].

Current opening across the kinematically complex southern Red Sea rift is constrained with relatively high-density GPS [e.g., *ArRajehi et al.*, 2010; *McClusky et al.*, 2010] and InSAR measurements [e.g., *Pagli et al.*, 2014]. These data show that south of ~16°N, the rift bifurcates into two branches: the main Red Sea and the subaerial Red Sea rift in Afar (Danakil Depression). Partitioning of extension between rift branches varies along strike. North of ~ 16°N, all the extension is accommodated in the main Red Sea rift, spreading at ~15 mm/yr. Moving south of 16°N, the extension is progressively accommodated in the Afar Depression reaching ~20 mm/yr at 13°N [*McClusky et al.*, 2010; *Vigny et al.*, 2006]. The crust beneath Afar varies from 25 km thick beneath most of Afar to 15 km thick beneath the Danakil Depression (Afdera-Erta'Ale segment) in the north [*Makris and Ginzburg*, 1987; *Bastow and Keir*, 2011] (Figure 1). The crustal thickness is ~25 km thick beneath the Danakil Block and increases to 40–45 km beneath the Ethiopian and Yemeni Plateaus [*Hammond et al.*, 2011; *Ahmed et al.*, 2013] (Figure 1).

2. Data

Our data set is based on continuous recordings from 89 seismic stations. Only a limited number of high-quality permanent seismic stations span the Afar-southern Red Sea margins, and so temporary experiments

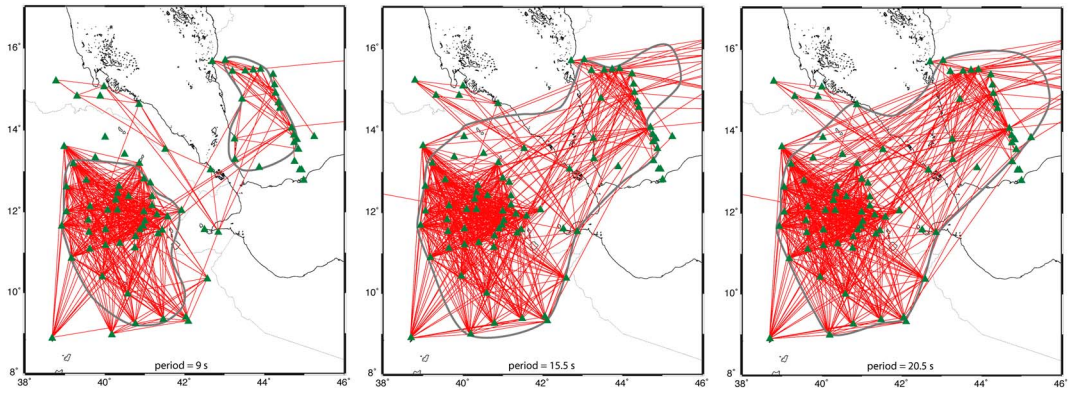

Figure 2. Map of the station pairs used for the tomographic inversion. The red lines show the station-to-station paths. The solid gray line delimitates the best constrained area. The green triangles are the stations.

using portable broadband equipment are our major source of information on the structure of the area. A seismic deployment was conducted between March 2009 and March 2010 as part of the YOCMAL (Young Conjugate Margins Laboratory) project, with 23 stations covering western Yemen during 1 year [*Korostelev et al.*, 2014; *Corbeau et al.*, 2014] (Figure 2). We also use data from 41 stations in the Afar Consortium network (UK and U.S., from March 2007 to November 2009) [e.g., *Keir et al.*, 2011], five stations of the Horn of Africa network in Yemen and Ethiopia (from June 1999 to December 2002 [e.g., *Sicilia et al.*, 2008]), and six temporary stations recording from May 2011 to September 2012 in Eritrea [e.g., *Hammond et al.*, 2013] (Figure 2]. One station from the Djibouti temporary network was added to our data set, together with permanent seismic stations in Djibouti, Yemen, and Ethiopia.

The ambient noise cross-correlation technique relies on having simultaneous recordings of the noise field at two seismic stations so that the Green's function between them can be estimated [*Shapiro and Campillo*, 2004; *Wapenaar and Fokkema*, 2006; *Halliday and Curtis*, 2008]. Because the different deployments of portable instruments occurred at different times, we are not able to estimate Green's functions for all receiver pairs. We partly compensate for this, however, by utilizing permanent stations from the IRIS and GEOSCOPE networks, providing data over a period during which several of the mentioned portable arrays were active.

3. Method

The ambient noise technique to study Earth structure is free of limitations imposed by the distribution of natural earthquakes. Extracting travel times from a multitude of station-station correlations therefore allows for relatively high-resolution tomographic inversions [e.g., *Shapiro et al.*, 2005]. We follow the approach of *Ekström et al.* [2009], discussed in further detail in section 3.2 of *Boschi et al.* [2013], to estimate phase velocity from the ambient signal recorded at two stations.

The background seismic noise is to a large extent generated by the coupling of oceans with the solid Earth [e.g., *Longuet-Higgins*, 1950; *Hillers et al.*, 2012]. Because this area is almost surrounded by seas or oceans (Red Sea, Gulf of Aden, and Indian Ocean), it is particularly suitable for ambient noise surface wave retrieval.

To maximize data quality, we (i) only used the pairs of stations that recorded simultaneously for at least 6 months and (ii) compared measured and predicted Green's function for all station pairs, and discarded pairs that clearly showed a bad fit (see figure in supporting information). The duration of cross-correlated signal varies by 6–36 months depending on the station pair. These long durations guarantee that all seasons and hence all possible azimuths of noise propagation are sampled [e.g., *Stehly et al.*, 2006]. Data processing was limited to whitening, as reasonable dispersion curves could be obtained without any filtering and/or "one-bit" amplitude compression.

4. Resolution

4.1. Station-to-Station Paths

To assess the resolving power of our inversion, we first show in Figure 2 the station-to-station paths corresponding to ambient Rayleigh wave observations at each period. The solid gray line delimitates the area with good coverage, and therefore the zone of best resolution.

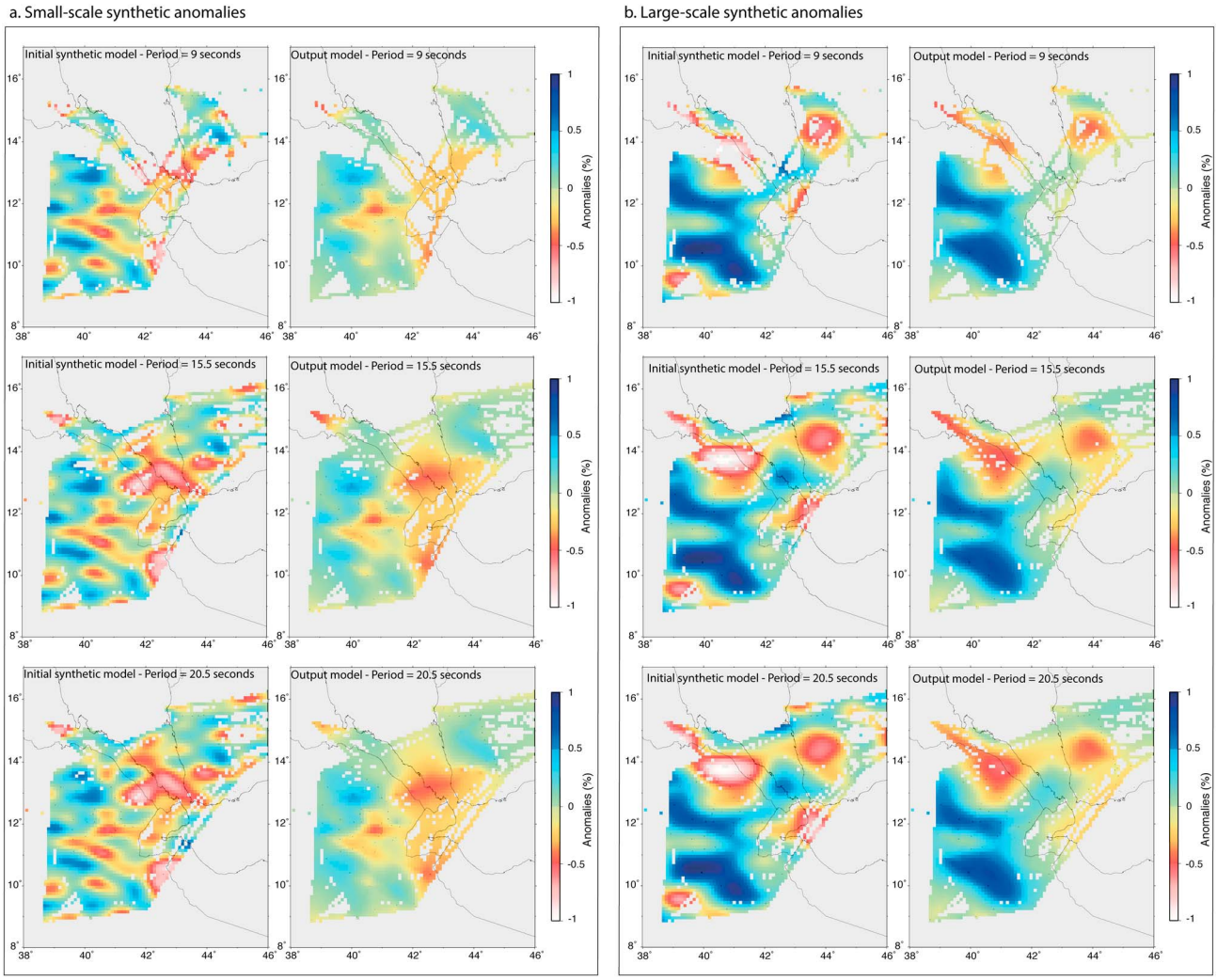

Figure 3. Result of two reconstruction synthetic tests with randomly distributed velocity anomalies of various sizes as input. (a) Small-scale synthetic anomalies and (b) large-scale synthetic anomalies. The left image displays the synthetic input, whereas the right image displays the output model.

4.2. Random Tests

We perform two random resolution tests [e.g., *Verbeke et al.*, 2012] to assess the reliability of the tomographic inversion: one with structures smaller than 100 km (Figure 3a) and a second one with structures larger than 100 km (Figure 3b). The input synthetic random velocity model consists of alternating random structures of opposite sign with a maximum velocity variation of 1.5% relative to the reference velocity.

Synthetic phase velocities were computed between the same station pairs as in the observed database. Figures 3a and 3b show the input velocity models and the retrieved velocity models from these tests for periods of 9, 15.5, and 20.5 s. These synthetic tests indicate that our inversion can resolve most of the Afar-southern Red Sea margins region, with some degradation of the recovered solutions near the edges of the illuminated area. The tomography algorithm is that utilized, e.g., by *Verbeke et al.* [2012]. Pixel size is $0.1° \times 0.1°$.

Our synthetic tests (Figure 3) serve both to validate pixel size and to select the values of regularization parameters that allow us to represent heterogeneities of scale length such as in Figure 3a (left). The same parameterization and regularization are applied to real data in the following. Notice that resolution changes across the region of study, so that a unique resolution limit cannot be specified.

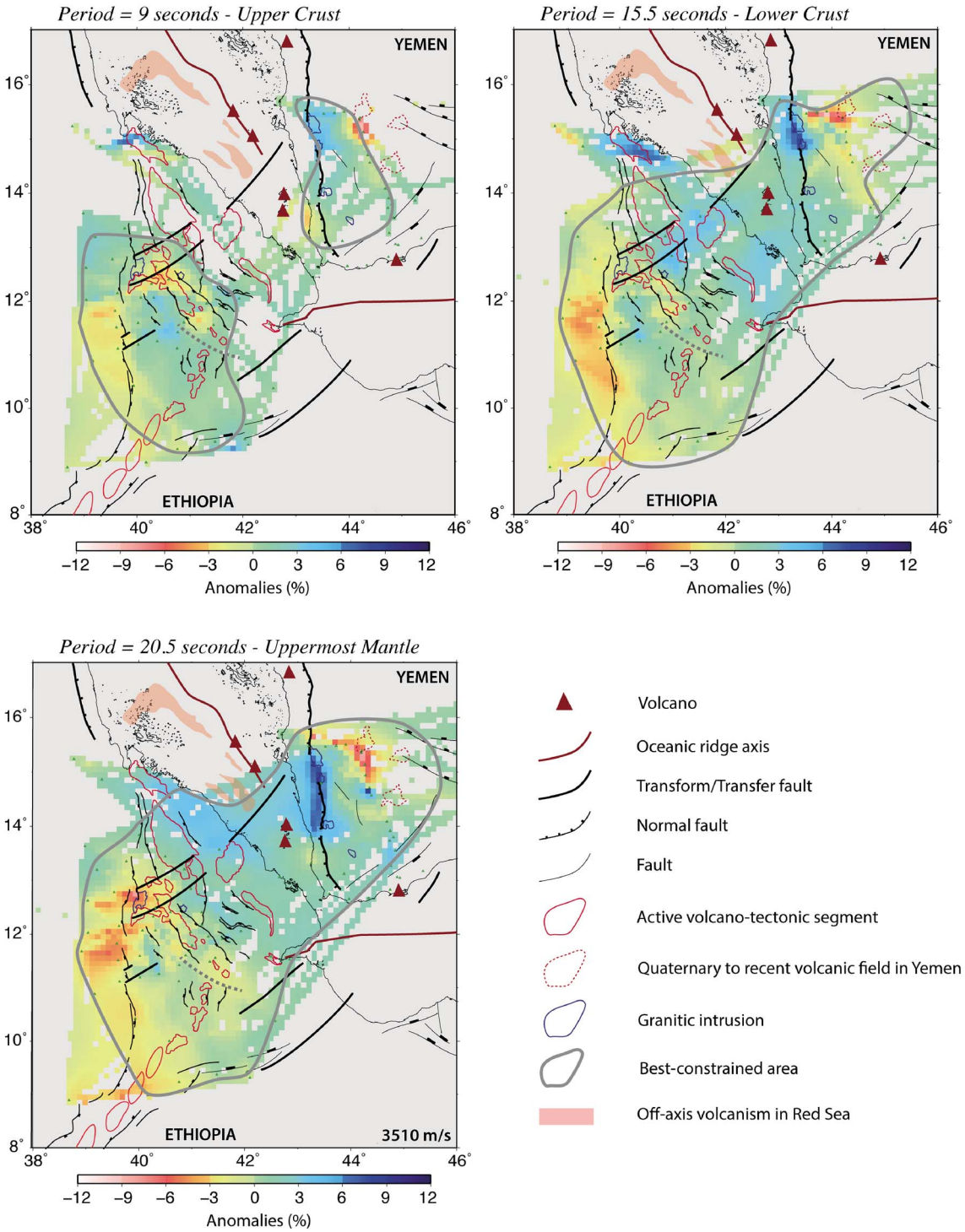

Figure 4. Maps of phase velocity anomalies (percent with respect to average) resulting from tomographic inversion of ambient noise dispersion data. The average velocity for each period is in the bottom right of each map (m/s). The solid gray line delimitates the best constrained area.

5. Results

We compute Rayleigh wave phase velocity maps for periods between 9 s and 25.5 s and present examples at 9, 15.5, and 20.5 s (Figure 4; see supporting information for other periods). According to, e.g., *Lebedev and Van Der Hilst* [2008] and *Fry et al.* [2010], 9 s Rayleigh waves are most sensitive to depths < 20 km (upper and middle crust), while 15.5 s are most sensitive to 10–40 km depth (primarily the lower crust). Rayleigh waves

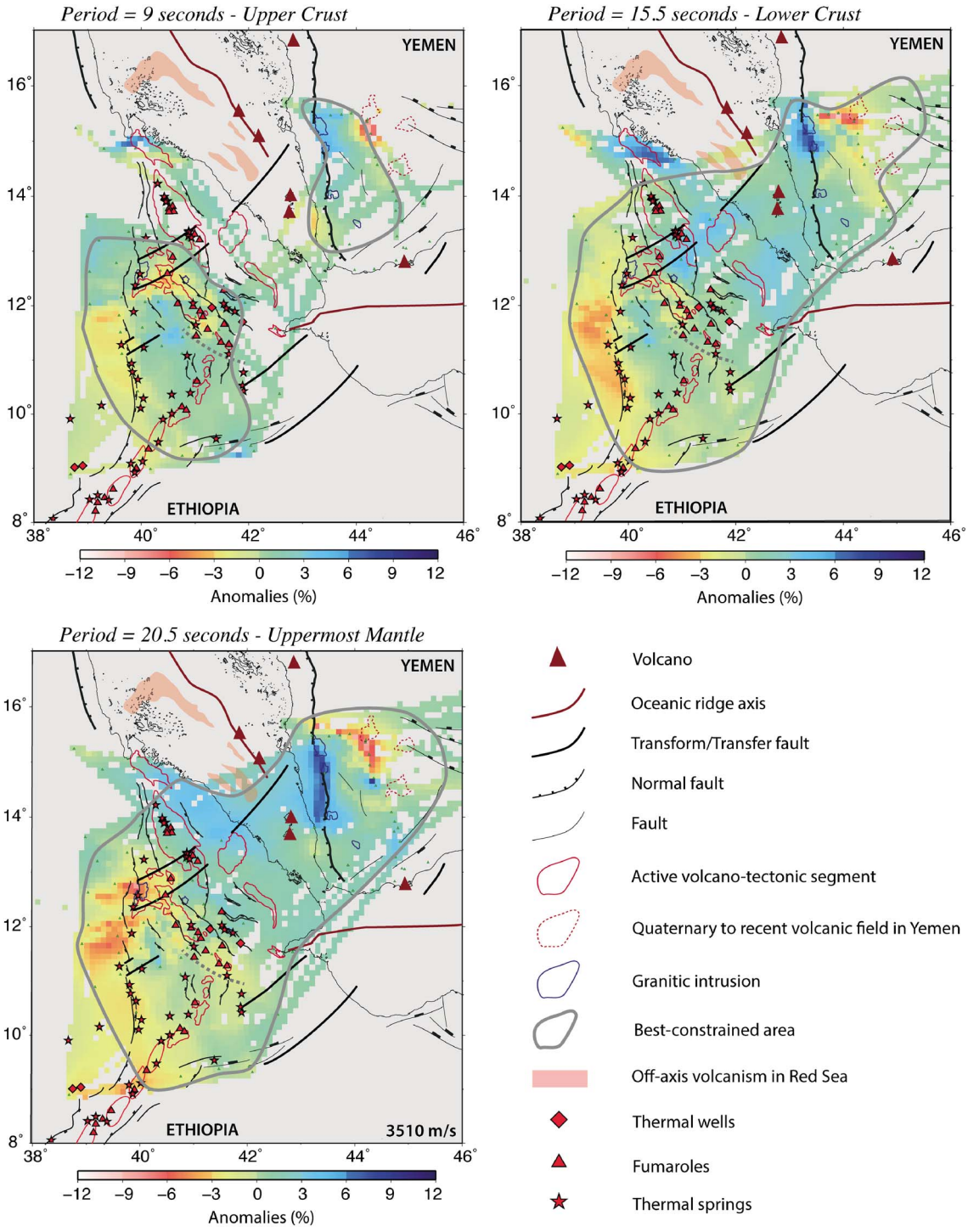

Figure 5. Distribution of thermal wells, fumaroles, and thermal springs in the Afar triple junction region [*Keir et al.*, 2009]. No data were available in Yemen.

of 20.5 s can sample down to 70 km, at the top of the upper mantle. The locus of major velocity anomalies is fairly constant from 9 s to 15.5 s (Figure 4). We image positive velocity perturbations beneath the border faults of the eastern flank of the Red Sea in Yemen, beneath the Danakil Horst, and in central western Afar in the region between the rift margin and the axial volcanic segments (Sullu Adu area, Figure 1). We also see positive velocity perturbations beneath the western Afar margin north of 12°N. The main slow anomalies are located beneath Dabbahu Manda-Hararo axial volcanic system, beneath Durrie off-axis volcano and the southern axis extension to Kurub Volcano (Figure 1). We also find slow anomalies associated with the

volcanic systems 150 to 200 km east of the rift margin in Yemen and beneath the western Afar margin south of 12°N (Figure 4).

The magnitude of several of the distinct velocity perturbations varies subtly with period. For example, beneath the eastern rift margin (Tihama Plain, Yemen, Figure 1), the positive anomaly increases in magnitude from 5% at 9 s to 7% at 20.5 s (Figure 4). The slow anomaly beneath the western Afar margin flank south of 12°N is mostly more than −3% at 9 s, whereas at 15.5 and 20.5 s a larger proportion of the anomaly is −4 to −6% (Figure 4).

The slow anomalies beneath Yemen and beneath the axial volcanic segment of Dabbahu-Manda-Hararo in Afar correlate well with the locus of surface volcanism (Figure 4). In addition, Figure 5 shows the surface distribution of known thermal springs in the region [*Keir et al.*, 2009]. The slow anomaly beneath the western Afar margin is beneath the locus of thermal springs on the western Afar margin, whereas north of 12°N, thermal springs are absent and the crust is faster than average. The spatial extent of slow anomalies imaged using ambient noise also correlates well with the spatial extent of high V_P/V_S ratios in the crust constrained using *P-S* receiver functions [*Hammond et al.*, 2011].

6. Discussion

Seismic wave velocity is known to be affected by the temperature and chemical composition of the medium of propagation (crustal rocks), as well as by the concentration of fluids, such as partial melt that might be present within crustal rocks [e.g., *Christensen and Mooney*, 1995; *Karato et al.*, 2003]. We image slow velocities beneath axial regions of localized magma intrusion, consistent with the hypothesis that major surface wave slow anomalies are associated with magmatism (Figure 4). In addition, the lowest velocities in our images are beneath zones of active volcanism and geothermal activity near the flanks of the southern Red Sea conjugate margins (Figures 4 and 5). The magnitude of the anomalies and spatial association with regions where either partial melt or fluids released from cooling magmatic systems are present suggests the crust beneath the flanks of the rift is currently being modified by magmatic processes. Ongoing magmatism occurs at the rift flanks in spite of the majority of strain having shifted to the rift axis since the onset of rifting at 11 Ma [*Wolfenden et al.*, 2004]. Beneath the western Afar margin, where slow anomalies are associated with geothermal systems rather than known volcanoes, geological studies suggest early border faulting at 30 Ma was associated with spatially localized volcanism in the marginal graben systems [*Ayalew et al.*, 2006]. Our velocity maps suggest that the magmatic systems beneath the rift flanks that were active during the onset of rifting remain magmatically active throughout the breakup process either through continued minor accumulation of partial melt in reservoirs, dike intrusion, and/or ongoing conductive cooling leading to release of fluids such as water [*Keir et al.*, 2009; *Holtzman and Kendall*, 2010].

The low-velocity anomalies in our phase velocity maps under the rift axis are observed with higher amplitude in the upper crust (Figure 4, period = 9 s), whereas the low-velocity anomalies located beneath the rift flanks are observed both in the upper and lower crust, but with higher amplitude in the lower crust (Figure 4, period = 15.5 s). This is consistent with the proposed plumbing systems of axial and flank volcanic systems of the nearby Main Ethiopian Rift, where petrological constraints on flank volcanism are good. The volcanic products observed on the flanks and at the axis of the Main Ethiopian Rift are not identical: they consist mainly of trachytes for the flanks and mainly of rhyolites and basalts for the axis [*Peccerillo et al.*, 2007]. Petrological models indicate that the origin of the off-axis trachytes is probably high-pressure fractional crystallization of asthenosphere-derived basalts, with this fractionation occurring at the base of the crust [*Peccerillo et al.*, 2007]. *Rooney et al.* [2005, 2007] suggest that these off-axis volcanic products result of moderate-degree partial melting at 50–90 km depth and undergo fractional crystallization in complex plumbing systems spanning depths throughout the crust [*Rooney et al.*, 2011]. The volcanic rocks at the axis are asthenospheric basalts produced by rift-related decompressional melting rather than other potential sources such as melting in the crust. The axial basalts undergo fractional crystallization mostly in the upper crust [*Peccerillo et al.*, 2007]. Thus, the axial magmatic chamber is shallow (in the upper crust), and the melt ascension from the asthenosphere is probably rapid. At the flanks, however, there is a complex plumbing system with stacked reservoirs both in the upper and lower crust [*Rooney et al.*, 2011]. The geothermal systems of the flanks are probably fed or heated by such a complex plumbing system (Figure 5). Our surface wave velocity maps are consistent with this model and therefore suggest similar magmatic plumbing systems for the southernmost Red Sea.

According to *Medynski et al.* [2015], the magma supply has decreased in the Dabbahu-Manda-Hararo axis reservoir since 15 kyr. An off-axis reservoir, located 15 km to the west of the Dabbahu-Manda-Hararo rift beneath Durrie Volcano has been actively fed since 15 kyr and is currently imaged using magneto-telluric techniques (Figure 1) [*Desissa et al.*, 2013]. It is consistent with our phase velocity maps, where the maximum amplitude for the northern Dabbahu-Manda-Hararo seems to be slightly to the west of the rift, beneath Durrie Volcano (Figure 4).

In the past, geodynamic models of breakup ignored the presence and impact of maintained magmatism at rift flanks on the thermal and subsidence history of the rift during late stage breakup and early seafloor spreading. At the southern Red Sea, where seafloor spreading is young, our new crustal velocity maps coupled with surface expression of volcanism (Figure 4) show clear evidence for ongoing magmatism beneath the rift flanks in Afar and Yemen (Sana'a, Dhamar, and Marib volcanic fields, Figure 1) [*Korostelev et al.*, 2014; *Corbeau et al.*, 2014]. Similarly, there is evidence for ongoing dike intrusion further north along the eastern Red Sea flank from InSAR (interferometric synthetic aperture radar) and seismicity studies at Harrat Lunayyir volcanic system in Saudi Arabia [e.g., *Pallister et al.*, 2010; *Ebinger et al.*, 2010]. There, localized subsidence, horizontal opening, and earthquakes in April to May 2009 are best modeled by intrusion of a dike and induced normal faulting. These studies, combined with the evidence presented by our new surface wave velocity maps, demonstrate that rift flank magmatism during late-stage breakup may be more common than previously assumed.

7. Conclusions

Our study provides new high-resolution phase velocity maps of the crust and uppermost mantle of the conjugate margins of the southern Red Sea (Afar and Yemen) using ambient noise tomography to constrain crustal evolution during breakup. Low-velocity anomalies are not only imaged in the crust beneath the axial volcanic systems but also in the upper and lower crust beneath rift flanks where hydrothermal activity and ongoing volcanism are observed at the surface. Our results show that the crust beneath the southern Red Sea Rift flanks is currently being modified by magmatic processes and that this activity is continuous from the onset of rifting. We therefore demonstrate that rift flank magmatism after breakup may be more common than it was previously thought in context of margins with excess magmatism.

Acknowledgments

This project was funded by the ANR-07-BLAN-0135 YOCMAL, CNRS-INSU-PICS Yemen, and GSMRB Yemen and is in the framework of the Actions Marges program. Seismic equipment from SEIS-UK is funded by NERC under agreement R8/H10/64. We thank David Hawthorn, Alex Brisbourne, and Victoria Lane for their efforts during the deployment and servicing of network, the French Embassy in Yemen, local governors, and the people of the Yemen governorates for their help during the field work. The authors thank Raphael Pik, Nicolas Bellahsen, and Martin Stab for discussions about the Afar region. D.K. is supported by NERC grant NE/L013932/1. C.W. is supported by the Netherlands Research Centre for Integrated Solid Earth Science (ISES). Djibouti instruments belong to the French National Pool of portable seismic instruments Sismob-RESIF and IPGS/EOST (University of Strasbourg).

The Editor thanks Piero Poli and an anonymous reviewer for their assistance evaluating this paper.

References

Ahmed, A., C. Tiberi, S. Leroy, G. W. Stuart, D. Keir, J. Sholan, K. Khanbari, I. Al-Ganad, and C. Basuyau (2013), Crustal structure of the rifted volcanic margins and uplifted plateau of Western Yemen from receiver function analysis, *Geophys. J. Int.*, *193*(3), 1673–1690.

ArRajehi, A., et al. (2010), Geodetic constraints on present-day motion of the Arabian Plate: Implications for Red sea and Gulf of Aden rifting, *Tectonics*, *29*, TC3011, doi:10.1029/2009TC002482.

Ayalew, D., C. Ebinger, E. Bourdon, E. Wolfenden, G. Yirgu, and N. Grassineau (2006), Temporal compositional variation of syn-rift rhyolites along the western margin of the southern Red Sea and northern Main Ethiopian Rift, *Geol. Soc. London Spec. Publ.*, *259*(1), 121–130.

Bastow, I. D., and D. Keir (2011), The protracted development of the continent-ocean transition in Afar, *Nat. Geosci.*, *4*(4), 248–250.

Boschi, L., C. Weemstra, J. Verbeke, G. Ekström, A. Zunino, and D. Giardini (2013), On measuring surface wave phase velocity from station–station cross-correlation of ambient signal, *Geophys. J. Int.*, *192*(1), 346–358.

Bosworth, W., P. Huchon, and K. McClay (2005), The Red Sea and Gulf of Aden Basins, *J. Afr. Earth. Sci.*, *43*(1–3), 334–378.

Christensen, N. I., and W. D. Mooney (1995), Seismic velocity structure and composition of the continental crust: A global view, *J. Geophys. Res.*, *100*(B6), 9761–9788.

Corbeau, J., F. Rolandone, S. Leroy, A. Al-Lazki, D. Keir, G. Stuart, and A. Stork (2014), Uppermost mantle velocity from Pn tomography in the Gulf of Aden, *Geosphere*, *10*(5), 958–968.

Daniels, K., I. Bastow, D. Keir, R. Sparks, and T. Menand (2014), Thermal models of dyke intrusion during development of continent–ocean transition, *Earth Planet. Sci. Lett.*, *385*, 145–153.

Desissa, M., N. Johnson, K. Whaler, S. Hautot, S. Fisseha, and G. Dawes (2013), A mantle magma reservoir beneath an incipient mid-ocean ridge in Afar, Ethiopia, *Nat. Geosci.*, *6*(10), 861–865.

Drake, C. L., and R. Girdler (1964), A geophysical study of the Red Sea, *Geophys. J. Int.*, *8*(5), 473–495.

Ebinger, C., and M. Casey (2001), Continental breakup in magmatic provinces: An Ethiopian example, *Geology*, *29*(6), 527–530.

Ebinger, C., D. Keir, A. Ayele, E. Calais, T. Wright, M. Belachew, J. Hammond, E. Campbell, and W. Buck (2008), Capturing magma intrusion and faulting processes during continental rupture: Seismicity of the Dabbahu (Afar) Rift, *Geophys. J. Int.*, *174*(3), 1138–1152.

Ebinger, C., A. Ayele, D. Keir, J. Rowland, G. Yirgu, T. Wright, M. Belachew, and I. Hamling (2010), Length and timescales of rift faulting and magma intrusion: The Afar rifting cycle from 2005 to present, *Annu. Rev. Earth Planet. Sci.*, *38*, 439–466.

Egloff, F., R. Rihm, J. Makris, Y. Izzeldin, M. Bobsien, K. Meier, P. Junge, T. Noman, and W. Warsi (1991), Contrasting structural styles of the eastern and western margins of the southern Red Sea: The 1988 SONNE experiment, *Tectonophysics*, *198*(2), 329–353.

Ekström, G., G. A. Abers, and S. C. Webb (2009), Determination of surface-wave phase velocities across USArray from noise and Aki's spectral formulation, *Geophys. Res. Lett.*, *36*, L18301, doi:10.1029/2009GL039131.

Ferguson, D. J., J. Maclennan, I. Bastow, D. Pyle, S. Jones, D. Keir, J. Blundy, T. Plank, and G. Yirgu (2013), Melting during late-stage rifting in Afar is hot and deep, *Nature*, *499*(7456), 70–73.

Fry, B., F. Deschamps, E. Kissling, L. Stehly, and D. Giardini (2010), Layered azimuthal anisotropy of Rayleigh wave phase velocities in the European Alpine lithosphere inferred from ambient noise, *Earth Planet. Sci. Lett.*, *297*(1), 95–102.

Grandin, R., A. Socquet, E. Jacques, N. Mazzoni, J.-B. de Chabalier, and G. King (2010), Sequence of rifting in Afar, Manda-Hararo rift, Ethiopia, 2005–2009: Time-space evolution and interactions between dikes from interferometric synthetic aperture radar and static stress change modeling, *J. Geophys. Res.*, *115*, B10413, doi:10.1029/2009JB000815.

Grandin, R., E. Jacques, A. Nercessian, A. Ayele, C. Doubre, A. Socquet, D. Keir, M. Kassim, A. Lemarchand, and G. King (2011), Seismicity during lateral dike propagation: Insights from new data in the recent Manda Hararo–Dabbahu rifting episode (Afar, Ethiopia), *Geochem. Geophys. Geosyst.*, *12*, Q0AB08, doi:10.1029/2010GC003434.

Halliday, D., and A. Curtis (2008), Seismic interferometry, surface waves and source distribution, *Geophys. J. Int.*, *175*(3), 1067–1087.

Hammond, J., J.-M. Kendall, G. Stuart, D. Keir, C. Ebinger, A. Ayele, and M. Belachew (2011), The nature of the crust beneath the Afar triple junction: Evidence from receiver functions, *Geochem. Geophys. Geosyst.*, *12*, Q12004, doi:10.1029/2011GC003738.

Hammond, J., et al. (2013), Mantle upwelling and initiation of rift segmentation beneath the Afar Depression, *Geology*, *41*(6), 635–638.

Hayward, N., and C. Ebinger (1996), Variations in the along-axis segmentation of the Afar Rift system, *Tectonics*, *15*(2), 244–257.

Hillers, G., N. Graham, M. Campillo, S. Kedar, M. Landès, and N. Shapiro (2012), Global oceanic microseism sources as seen by seismic arrays and predicted by wave action models, *Geochem. Geophys. Geosyst.*, *13*, Q01021, doi:10.1029/2011GC003875.

Holtzman, B. K., and J.-M. Kendall (2010), Organized melt, seismic anisotropy, and plate boundary lubrication, *Geochem. Geophys. Geosyst.*, *11*, Q0AB06, doi:10.1029/2010GC003296.

Karato, S. I., et al. (2003), *The Dynamic Structure of the Deep Earth: An Interdisciplinary Approach*, Princeton Univ. Press, Princeton. N. J.

Keir, D., I. Bastow, K. Whaler, E. Daly, D. Cornwell, and S. Hautot (2009), Lower crustal earthquakes near the Ethiopian Rift induced by magmatic processes, *Geochem. Geophys. Geosyst.*, *10*, Q0AB02, doi:10.1029/2009GC002382.

Keir, D., C. Pagli, I. Bastow, and A. Ayele (2011), The magma-assisted removal of Arabia in Afar: Evidence from dike injection in the Ethiopian Rift captured using InSAR and seismicity, *Tectonics*, *30*, TC2008, doi:10.1029/2010TC002785.

Korostelev, F., et al. (2014), Crustal and upper mantle structure beneath south-western margin of the Arabian Peninsula from teleseismic tomography, *Geochem. Geophys. Geosyst.*, *15*, 2850–2864, doi:10.1002/2014GC005316.

Laughton, A., and C. Tramontini (1969), Recent studies of the crustal structure in the Gulf of Aden, *Tectonophysics*, *8*(4), 359–375.

Lebedev, S., and R. D. Van Der Hilst (2008), Global upper-mantle tomography with the automated multimode inversion of surface and *S*-wave forms, *Geophys. J. Int.*, *173*(2), 505–518.

Leroy, S., et al. (2010), Contrasted styles of rifting in the eastern Gulf of Aden: A combined wide-angle, multichannel seismic, and heat flow survey, *Geochem. Geophys. Geosyst.*, *11*, Q07004, doi:10.1029/2009GC002963.

Longuet-Higgins, M. S. (1950), A theory of the origin of microseisms, *Philos. Trans. R. Soc. London, Ser. A*, *243*(857), 1–35.

Maccaferri, F., E. Rivalta, D. Keir, and V. Acocella (2014), Off-rift volcanism in rift zones determined by crustal unloading, *Nat. Geosci.*, *7*, 297–300.

Makris, J., and A. Ginzburg (1987), The Afar Depression: Transition between continental rifting and sea-floor spreading, *Tectonophysics*, *141*(1), 199–214.

Manetti, P., G. Capaldi, S. Chiesa, L. Civetta, S. Conticelli, M. Gasparon, L. Volpe, and G. Orsi (1991), Magmatism of the eastern Red Sea margin in the northern part of Yemen from Oligocene to present, *Tectonophysics*, *198*(2), 181–202.

McClusky, S., et al. (2010), Kinematics of the southern Red Sea–Afar Triple Junction and implications for plate dynamics, *Geophys. Res. Lett.*, *37*, L05301, doi:10.1029/2009GL041127.

Medynski, S., et al. (2015), Stability of rift axis magma reservoirs: Spatial and temporal evolution of magma supply in the dabbahu rift segment (Afar, Ethiopia) over the past 30 kyr, *Earth Planet. Sci. Lett.*, *409*, 278–289.

Pagli, C., H. Wang, T. J. Wright, E. Calais, and E. Lewi (2014), Current plate boundary deformation of the Afar rift from a 3-D velocity field inversion of InSAR and GPS, *J. Geophys. Res. Solid Earth*, *119*, 8562–8575, doi:10.1002/2014JB011391.

Pallister, J., et al. (2010), Broad accommodation of rift-related extension recorded by dyke intrusion in Saudi Arabia, *Nat. Geosci.*, *3*(10), 705–712.

Peccerillo, A., C. Donati, A. Santo, A. Orlando, G. Yirgu, and D. Ayalew (2007), Petrogenesis of silicic peralkaline rocks in the Ethiopian Rift: Geochemical evidence and volcanological implications, *J. Afr. Earth. Sci.*, *48*(2), 161–173.

Prodehl, C., and J. Mechie (1991), Crustal thinning in relationship to the evolution of the Afro-Arabian rift system: A review of seismic-refraction data, *Tectonophysics*, *198*(2), 311–327.

Reed, C. A., S. Almadani, S. S. Gao, A. A. Elsheikh, S. Cherie, M. G. Abdelsalam, A. K. Thurmond, and K. H. Liu (2014), Receiver function constraints on crustal seismic velocities and partial melting beneath the Red Sea Rift and adjacent regions, Afar Depression, *J. Geophys. Res. Solid Earth*, *119*, 2138–2152, doi:10.1002/2013JB010719.

Rooney, T., T. Furman, I. Bastow, D. Ayalew, and G. Yirgu (2007), Lithospheric modification during crustal extension in the Main Ethiopian Rift, *J. Geophys. Res.*, *112*, B10201, doi:10.1029/2006JB004916.

Rooney, T., I. Bastow, and D. Keir (2011), Insights into extensional processes during magma assisted rifting: Evidence from aligned scoria cones, *J. Volcanol. Geotherm. Res.*, *201*(1–4), 83–96.

Rooney, T., C. Herzberg, and I. Bastow (2012), Elevated mantle temperature beneath East Africa, *Geology*, *40*(1), 27–30.

Rooney, T. O., T. Furman, G. Yirgu, and D. Ayalew (2005), Structure of the Ethiopian lithosphere: Xenolith evidence in the Main Ethiopian Rift, *Geochim. Cosmochim. Acta*, *69*(15), 3889–3910.

Rooney, T. O., I. D. Bastow, D. Keir, F. Mazzarini, E. Movsesian, E. B. Grosfils, J. R. Zimbelman, M. S. Ramsey, D. Ayalew, and G. Yirgu (2014), The protracted development of focused magmatic intrusion during continental rifting, *Tectonics*, *33*, 875–897, doi:10.1002/2013TC003514.

Ruegg, J. (1975), Main results about the crustal and upper mantle structure of the Djibouti region (TFAI), *Afar Depression of Ethiopia*, *1*, 120–134.

Shapiro, N. M., and M. Campillo (2004), Emergence of broadband Rayleigh waves from correlations of the ambient seismic noise, *Geophys. Res. Lett.*, *31*, L07614, doi:10.1029/2004GL019491.

Shapiro, N. M., M. Campillo, L. Stehly, and M. H. Ritzwoller (2005), High-resolution surface-wave tomography from ambient seismic noise, *Science*, *307*(5715), 1615–1618.

Sicilia, D., et al. (2008), Upper mantle structure of shear-waves velocities and stratification of anisotropy in the Afar hotspot region, *Tectonophysics*, *462*(1–4), 164–177.

Stab, M., N. Bellahsen, R. Pik, S. Leroy, and D. Ayalew (2014), Mode of rifting in magmatic-rich setting: Tectono-magmatic evolution of the central afar rift system, in *EGU General Assembly Conference Abstracts, Vienna, Austria*, vol. 16, 14,484 pp.

Stehly, L., M. Campillo, and N. Shapiro (2006), A study of the seismic noise from its long-range correlation properties, *J. Geophys. Res.*, *111*, B10306, doi:10.1029/2005JB004237.

Tramontini, C., and D. Davies (1969), A seismic refraction survey in the Red Sea, *Geophys. J. Int.*, *17*(2), 225–241.

Verbeke, J., L. Boschi, L. Stehly, E. Kissling, and A. Michelini (2012), High-resolution Rayleigh-wave velocity maps of central Europe from a dense ambient-noise data set, *Geophys. J. Int.*, *188*(3), 1173–1187.

Vigny, C., P. Huchon, J.-C. Ruegg, K. Khanbari, and L. M. Asfaw (2006), Confirmation of Arabia plate slow motion by new GPS data in Yemen, *J. Geophys. Res.*, *111*, B02402, doi:10.1029/2004JB003229.

Wapenaar, K., and J. Fokkema (2006), Green's function representations for seismic interferometry, *Geophysics*, *71*(4), SI33–SI46.

Wolfenden, E., C. Ebinger, G. Yirgu, A. Deino, and D. Ayalew (2004), Evolution of the northern Main Ethiopian Rift: Birth of a triple junction, *Earth Planet. Sci. Lett.*, *224*(1), 213–228.

Wolfenden, E., C. Ebinger, G. Yirgu, P. Renne, and S. Kelley (2005), Evolution of a volcanic rifted margin: Southern Red Sea, Ethiopia, *Geol. Soc. Am. Bull.*, *117*(7–8), 846–864.